Computers and Geosciences 126 (2019) 107–119

Contents lists available at ScienceDirect

Computers and Geosciences

journal homepage: www.elsevier.com/locate/cageo

COMPEST, a PEST-COMSOL interface for inverse multiphysics modelling: Development and application to isotopic fractionation of groundwater contaminants

Landon J.S. Halloran*, Philip Brunner, Daniel Hunkeler

Centre d'Hydrogéologie et de Géothermie (CHYN), Université de Neuchâtel, Switzerland

ARTICLE INFO

Keywords:
Inverse problems
Parameter estimation
Uncertainty analysis
Numerical environmental models
Hydrogeology
Contaminant hydrology

ABSTRACT

In the geosciences, inverse problems, wherein observations corresponding to model outputs are known and model parameters are unknown, are commonplace. Many of these problems involve coupled physical, chemical, and other processes that can be modelled using forward finite-element models. Here, we present a novel interface, COMPEST, that connects the parameter estimation and uncertainty analysis package, PEST, with the finite-element modelling package, COMSOL Multiphysics. To demonstrate some of the capabilities of this approach, we also develop and present a novel model for the degradation and transport of chlorohydrocarbons in low-permeability units. This model integrates isotopic fractionation arising from degradation and diffusion. Three implementations of this model with increasing complexity are used to demonstrate the functionality of the developed interface. This linkage provides a means for parameter estimation, uncertainty analysis, and singular value decomposition to gain insight into the behaviour, identifiability, and interdependence of the various parameters in the model. COMPEST is written so as to be suited to a wide range of scientific and engineering applications and thus can be used to link any COMSOL model with PEST. This enables the use of advanced inverse modelling techniques previously unavailable to COMSOL users.

1. Introduction

Coupled numerical modelling of multiple types of physical, chemical, and other processes is a powerful tool in the investigation of a wide range of geoscientific problems. While in certain domains of science and engineering, coupled numerical models may, to a high level of precision, simulate the behaviour of systems, in hydrogeology the sparseness of data and the inherent heterogeneity of the earth generally force us to use models in a subtly different way. The concept of the coupled numerical model functioning as a data processing tool–as opposed to a system simulator–is therefore commonplace. In any application where data is sparse or has measurement error, there will be uncertainty associated with any resulting prediction. In order to inform decisions and to obtain the highest value from a model, this uncertainty needs to be quantified. Furthermore, in highly parameterised models, the optimization problem may be ill-posed or difficult to solve, necessitating a certain class of inverse problem techniques in order to constrain the results (Tikhonov et al., 2013).

There exist several modelling packages which enable the modelling of multiple physical and chemical processes (for an overview, see Keyes et al., 2013). COMSOL Multiphysics (COMSOL, 2014) is a versatile finite element modelling package that enables the coupling of physical processes and offers model set-up via a high-level GUI. Several modules are offered for specific applications and, critically, any value or equation can be modified or introduced by the user. It has seen use in a diverse range of fields such as acoustics (e.g. Hammarström et al., 2010), fuel cell development (e.g. Sezgin et al., 2016), and chemical engineering (e.g. Wei and Weavers, 2016). In hydrology, the multiphysics modelling approach can address problems that involve both general, distributed groundwater issues and more unique, multidisciplinary problems (Li et al., 2009). COMSOL, in particular, has been used to investigate groundwater-surface water exchange (Chui and Freyberg, 2009; Halloran et al., 2017), groundwater dating (Cardenas, 2007; Gleeson et al., 2015), plume transport (Fjordboge et al., 2012), and groundwater-vegetation interactions (Lowry et al., 2011). Notably, this software has recently been interfaced with the discrete-element package YADE (Pirnia et al., 2018) and with the geochemistry packages PHREEQC (Nardi et al., 2014) and GEMS (Azad et al., 2016). While COMSOL offers basic parameter estimation functionality, it is otherwise lacking in its ability to quantify uncertainty, evaluate data worth, and

* Corresponding author. CHYN, Université de Neuchâtel, rue Émile-Argand 11, 2000, Neuchâtel, Switzerland.
E-mail address: landon.halloran@unine.ch (L.J.S. Halloran).

https://doi.org/10.1016/j.cageo.2019.02.001
Received 8 November 2018; Received in revised form 31 January 2019; Accepted 4 February 2019
Available online 16 February 2019
0098-3004/

treat highly parameterised models.

In the field of hydrology, and in hydrogeology in particular, the software package PEST (Doherty, 2015, 2016a) and associated packages, BeoPEST (Schreuder, 2009), PEST++ (Welter et al., 2015) and pyEMU (White et al., 2016), have been widely adopted to solve inverse problems using models. PEST is model-independent and can be used to estimate the values of given parameters, make predictions, calculate sensitivities and uncertainties, and evaluate the relevant value of observations. Application examples include parameter estimation ("model calibration") in geochemical (van Breukelen and Griffioen, 2004) and hydro-physical (Moeck et al., 2015) models, sensitivity analysis in watershed (Bahremand and De Smedt, 2008) and nutrient transport (Baginska et al., 2003) models, and predictive analysis in coupled hydrology-vegetation (Schilling et al., 2014) and water quality (Nolan et al., 2011) models. There is also increasing interest in using PEST to evaluate impacts on parameter uncertainty reduction by selected observations via data worth analysis (Wallis et al., 2014; Kikuchi, 2017).

While the range of scenarios that can be addressed by combining multiphysics finite-element modelling with inverse methods is extensive, we focus here on a set of problems involving the transport and degradation of chlorohydrocarbons in the subsurface. Chlorohydrocarbons are common groundwater contaminants (e.g. Elsner et al., 2010; Hunkeler et al., 2005) whose potential health effects are well documented (e.g., Scott and Cogliano, 2000; Lee et al., 2003). Typically, these contaminants enter the subsurface as dense non-aqueous phase liquids (DNAPLs) and are then slowly dissolved and transported via advective and diffusive flow. There exist many examples of remediation attempts–e.g., pump-and-treat (Mackay and Cherry, 1989), permeable reactive barriers (Obiri-Nyarko et al., 2014), nanoscale zero-valent iron (Crane and Scott, 2012), and thermal methods (Heron et al., 2016)–which often bear significant financial cost. Consequently, monitored natural attention (MNA) by microbiota present in the subsurface is frequently chosen for at least part of the duration of remediation efforts (Meckenstock et al., 2015). Crucially, chlorohydrocarbons have been observed to diffuse into aquitards (low permeability units) and subsequently back-diffuse into the overlying aquifer (Parker et al., 2008). This phenomenon can drastically lengthen the duration of plume persistence even when remediation efforts are undertaken (Seyedabbasi et al., 2012; Yang et al., 2017). Nevertheless, degradation can occur in the aquitard (Wanner et al., 2016) and therefore understanding the relevant reaction and transport dynamics is crucial for making predictions about contaminant fate.

In the subsurface, dechlorination (degradation in which Cl atoms are removed from the parent compound) of chlorohydrocarbons can occur biotically or abiotically and at a wide range of rates. Each molecule of a compound has several isotopologues that contain different proportions of isotopes of a given element (here, C and Cl). Due to the differences in bond strength, reaction kinetics of a given degradation step are dependent on the isotopes present in the molecule. This results in isotopic enrichment or depletion in the parent and daughter compounds, the degree of which depends on the dechlorination mechanism (Chapters 18 and 25 of Adrian and Löffler, 2016). This relative enrichment can be measured using compound-specific isotope analysis (CSIA) which can be used to provide information about the fate of groundwater contaminants (Meckenstock et al., 2004).

In this work, we present a framework that links PEST and COMSOL Multiphysics via a novel *java*-based interface, COMPEST. We also present the details of a model for isotopic enrichment during degradation of tetra-, tri-, and *cis*-di-chloroethene (PCE, TCE and *c*DCE, respectively). We demonstrate three implementations of this model, adding complexity in each subsequent implementation, to exhibit and evaluate some of the capabilities of the COMSOL-COMPEST-PEST set-up.

2. Theory

2.1. Parameter estimation and inverse problems

We present here a brief overview of parameter estimation theory for inverse modelling problems. For a deeper treatment refer to, e.g., Parker (1994), Cullen et al. (2013), or Doherty (2015).

One can consider a forward model to be a matrix function $\mathbf{X}$ (size $m \times n$) that transforms a vector of parameters $\vec{p}$ (length n) to a vector of observations $\vec{b}$ (length m):

$$\mathbf{X}\vec{p} + \vec{\varepsilon} = \vec{b} \tag{1}$$

where $\vec{\varepsilon}$ represents the uncertainty or error on each observation in $\vec{b}$. In many cases, this matrix function may be non-linear. In inverse modelling, the typical aim is to determine $\vec{p}$ given $\vec{b}$. If $m \leq n$, and $\mathbf{X}^{-1}$ exists, the problem may be well-posed. If measurement error is zero ($\vec{\varepsilon} = \vec{0}$) and $m = n$, $\vec{p}_{est}$, in this case sometimes called the "naïve inverse solution," can be determined exactly:

$$\vec{p}_{est} = \vec{p} = \mathbf{X}^{-1}\vec{b} \tag{2}$$

Using the same assumptions, but allowing $m < n$ and also assuming that $\mathbf{X}$ does not have a non-zero null space (i.e., $\nexists\, \vec{v} \neq \vec{0}$ such that $\mathbf{X}\vec{v} = \vec{0}$), we must multiply both sides of Equation (1) by $(\mathbf{X}^T\mathbf{X})^{-1}\mathbf{X}^T$ to obtain:

$$\vec{p} = (\mathbf{X}^T\mathbf{X})^{-1}\mathbf{X}^T\vec{b} \tag{3}$$

Clearly, the assumptions involved in the above are violated in many real-world applications. Measurement uncertainty is always present and the quantity of parameters to be determined in the inverse model may exceed the number of observations (i.e., $m > n$). This leads to the problem of parameter non-uniqueness, commonplace in hydrogeology and geophysics.

To take noise into account, we can define a weight matrix $\mathbf{Q}$:

$$\mathbf{Q} = \sigma_r^2 C^{-1}(\vec{\varepsilon}) \tag{4}$$

where σ_r^2 is a proportionality constant and $C(\vec{\varepsilon})$ is the diagonal covariance matrix describing uncertainty in observations $\vec{p}$. The residual vector $\vec{r} = \vec{b} - \mathbf{X}\vec{p}$ is the difference between observations and model outputs. As $\mathbf{Q}^{-1}\mathbf{Q} = \mathbf{I}$, we can define an objective function to be minimized in order to determine the optimized parameters $\vec{p}$ given observations $\vec{b}$:

$$\Phi = \vec{r}^T\mathbf{Q}\vec{r} = (\vec{b} - \mathbf{X}\vec{p})^T\mathbf{Q}(\vec{b} - \mathbf{X}\vec{p}) \tag{5}$$

By minimizing the objective function, we can obtain an estimate of the parameters $\vec{p}_{est}$ with an error of

$$\vec{p}_{est} - \vec{p} = (\mathbf{X}^T\mathbf{Q}\mathbf{X})^{-1}\mathbf{X}^T\mathbf{Q}\vec{\varepsilon} \tag{6}$$

which has a co-variance of

$$cov(\vec{p}_{est} - \vec{p}) = \sigma_r^2(\mathbf{X}^T\mathbf{Q}\mathbf{X})^{-1} \tag{7}$$

In practice, the behaviour of a non-linear model can be estimated linearly through evaluation of the Jacobian matrix

$$\mathbf{J} = \begin{bmatrix} \frac{\partial \vec{b}}{\partial p_1} & \cdots & \frac{\partial \vec{b}}{\partial p_n} \end{bmatrix} \tag{8}$$

which is substituted, along with residual vector $\vec{r}$, into Equation (6):

$$\vec{p}_{est} - \vec{p} = (\mathbf{J}^T\mathbf{Q}\mathbf{J})^{-1}\mathbf{J}^T\mathbf{Q}\vec{r} \tag{9}$$

Minimization of the objective function thus becomes an iterative process wherein $\mathbf{J}$ must be evaluated at each inverse modelling step.

Singular value decomposition (SVD) is a factorization method that

decomposes a matrix–in this case, the Jacobian–into three components:

$$\mathbf{J} = \mathbf{U}\mathbf{\Sigma}\mathbf{V}^{*} \tag{10}$$

Here, $\mathbf{U}$ and $\mathbf{V}$ are unitary matrices of sizes $m \times m$ and $n \times n$, respectively. $\mathbf{\Sigma}$ is a diagonal matrix (size $m \times n$) where the values on the diagonal, referred to as singular values, decrease with increasing index (i.e. $\Sigma_{i,i} > \Sigma_{i+1,i+1}$, etc.). This matrix decomposition technique allows singular values below a selected threshold to be discarded through matrix truncation, rendering calculations significantly more efficient, and is thus used in many compression algorithms and machine-learning applications (e.g., Andrews and Patterson, 1976; Zou and Shi, 2016). For inverse problems, SVD proves to be powerful in increasing the efficiency of numerical regularization and, in particular, in the treatment of problems where $n > m$ or where the behaviour of certain parameters is not fully independent. In this case, matrix truncation reduces the number of orthogonal, linear combinations of parameters in $\vec{p}$ (eigenvectors) to be estimated. The sum of the squares of these vectors for a given parameter is referred to as the identifiability, ξ. More formally, Doherty and Hunt (2009) define the identifiability of the j^{th} parameter as

$$\xi_j = (\mathbf{V}_1\mathbf{V}_1^{T})_{j,j} \tag{11}$$

where $\mathbf{V}_1$ is the truncated $\mathbf{V}$ matrix containing the selected eigenvectors. More extensive information on SVD can be found in, for example, Strang (2016), while Doherty (2016a) details its implementation in PEST.

A final relevant technique is the *Marquardt* lambda (λ) (*Gauss-Marquardt-Levenberg* method). This technique applies a dynamic damping factor to avoid parameter overshoot, thus reducing the number of model runs required for regularization. With the introduction of the *Marquardt* Lambda, which is decreased with each inverse modelling step, the estimate of parameter error (Equation (9)) becomes:

$$\vec{p}_{est} - \vec{p} = (\mathbf{J}^{T}\mathbf{Q}\mathbf{J} + \lambda\mathbf{I})^{-1}\mathbf{J}^{T}\mathbf{Q}\vec{r} \tag{12}$$

Jacobian evaluation, SVD, and the *Marquardt* λ are all implemented in PEST.

2.2. Isotope fractionation and CSIA

The behaviour of concentration C of a given species γ_i can be described by the convection-diffusion-degradation equation:

$$\frac{\partial(nC_{\gamma_i})}{\partial t} = \nabla\cdot(D_{\gamma_i}\nabla C_{\gamma_i}) - \vec{v}\cdot\nabla C_{\gamma_i} + \left[\frac{\partial C_{\gamma_i}}{\partial t}\right]_{\text{reactions}} \tag{13}$$

where D is the diffusion coefficient; n, porosity; and $\vec{v}$, the advective velocity. This equation, with isotopic fractionation implemented through the terms D (diffusion) and $[\partial C_{\gamma_i}/\partial t]_{\text{reactions}}$ (degradation and production), is implemented in the finite-element model.

Isotopologues are molecules of the same compound containing different proportions of isotopes of a given element (e.g., for water: $^{1}H^{16}O^{1}H$, $^{1}H^{18}O^{1}H$, etc.). Isotopic fractionation arises due to slight differences in the manifestations of various phenomena in each isotopologue. It can be caused by a variety of mechanisms. For contaminants in the saturated subsurface, degradation and, to a lesser extent, diffusion are the primary mechanisms for fractionation. Degradation involves the breaking of bonds in the parent molecule. As heavier isotopes generally have stronger bonds than their lighter counterparts, this results in a relative enrichment of heavy isotopes in the parent compound and a relative depletion in the daughter compound.

Diffusion can also contribute to varying isotopic profiles (LaBolle et al., 2008). The diffusion coefficient of a heavier molecule D_H is generally lower than that of a lighter one D_L, and can be approximated by the Chapman-Enskog relationship:

$$\frac{D_H}{D_L} = \sqrt{\frac{m_L^{*}}{m_H^{*}}} \tag{14}$$

where m^{*} denotes the reduced mass of a compound of molecular mass m in a given solvent of molecular mass m_{sol}:

$$m^{*} = 2\frac{m\cdot m_{sol}}{m + m_{sol}}. \tag{15}$$

Isotopic enrichment or depletion is generally given in per-mille (‰) terms in comparison to a reference value. For carbon:

$$\delta^{13}C = \left[\frac{\left(\frac{^{13}C}{^{12}C}\right)_{sample}}{\left(\frac{^{13}C}{^{12}C}\right)_{VPDB}} - 1\right] 1000‰ \tag{16}$$

and for chlorine:

$$\delta^{37}Cl = \left[\frac{\left(\frac{^{37}Cl}{^{35}Cl}\right)_{sample}}{\left(\frac{^{37}Cl}{^{35}Cl}\right)_{SMOC}} - 1\right] 1000‰ \tag{17}$$

where VPDB is the Vienna Pee Dee Belemnite standard (Coplen et al., 2006) and SMOC is the Standard Mean Ocean Chloride standard (Wei et al., 2012).

Compound-specific isotope analysis (CSIA) is the set of techniques used to measure the isotopic enrichment of a given element in a selected compound. The techniques involve the isolation of the selected compound and transformation to a measurement gas, followed by mass distribution analysis using a mass spectrometer (Schmidt et al., 2004; Meckenstock et al., 2004; Cincinelli et al., 2012). By measuring the relative distribution of molecular masses of a given compound, an estimate of isotopic enrichment can be made. CSIA has been a useful tool in identifying degradation pathways of chlorinated organic contaminants (e.g., Audí-Miró et al., 2013; Badin et al., 2016; Palau et al., 2017; Ponsin et al., 2017). For a given compound, each degradation pathway differs in its isotopic enrichment factor (ε) and, jointly, its kinetic isotope effect (KIE) (for an extensive discussion of these, see, for example Elsner et al., 2005; Elsner, 2010). To first-order, the kinetic isotope effect is defined as:

$$\text{KIE} = \frac{k_L}{k_H} \tag{18}$$

where k_L and k_H refer to the reaction (degradation) rate of the light and heavy versions of a given compound. Here, we focus on the apparent isotope effect (AKIE) A, which is the manifestation of the ensemble of relevant kinetic isotope effects measurable with CSIA. For the vast majority of reactions, including chlorohydrocarbon dechlorination, $A > 1$. Isotopic enrichment factors and apparent kinetic isotope effects have been measured for a number of organic and inorganic degradation pathways and the database of values continues to grow (Adrian and Löffler, 2016, Chapters 18 & 25). Enrichment factors can be converted to AKIEs by (Elsner et al., 2005):

$$A = \frac{1}{1 + z\varepsilon_{\text{reactive position}}/1000} \tag{19}$$

where z is the number of indistinguishable, reactive sites and $\varepsilon_{\text{reactive position}}$ is the enrichment factor corresponding to the reactive position.

For a simplified case considering only heavy (H) and light (L) versions of a parent compound (e.g., PCE with one ^{13}C vs. zero ^{13}C), the rate of change in concentration C due to reactions is:

$$\frac{\partial C_{\text{PCE}}}{\partial t} = \frac{\partial C_{\text{PCE}_H}}{\partial t} + \frac{\partial C_{\text{PCE}_L}}{\partial t} = -\alpha_{\text{PCE}_H}\frac{C_{\text{PCE}_H}}{C_{\text{PCE}}} - \alpha_{\text{PCE}_L}\frac{C_{\text{PCE}_L}}{C_{\text{PCE}}} \tag{20}$$

where α denotes the reaction rate of the individual isotope.

More generally, the total decay rate of compound γ is defined as R_γ and the total production rate as $R_{\gamma-1}$ (i.e., the total decay rate of compound $\gamma-1$). The rate of change in concentration of isotopologue γ_i as compound $\gamma-1$ is degraded to γ and compound γ is degraded to $\gamma+1$ is thus (adapted from Van Breukelen et al., 2005; Badin et al., 2018):

$$\frac{\partial C_{\gamma_i}}{\partial t} = \left[\sum_{h\in(\gamma-1)_{\text{iso}}} \kappa^{\gamma-1\to\gamma}_{\gamma_h,\gamma_i} R_{\gamma-1} \frac{C_{(\gamma-1)_h}}{C_{(\gamma-1)}}\right] - \left[\sum_{j\in(\gamma+1)_{\text{iso}}} \kappa^{\gamma\to\gamma+1}_{\gamma_i,\gamma_j}\right] R_\gamma \frac{C_{\gamma_i}}{C_\gamma} \tag{21}$$

Here, the rate of production of γ_i is determined by the first term and the rate of degradation by the second term. The terms $(\gamma-1)_{\text{iso}}$ and $(\gamma+1)_{\text{iso}}$ refer to the sets of isotopologues of the parent and daughter compounds, respectively. The κ matrices are the transition matrices which determine the relative amounts of each isotopologue in the parent compound $(\gamma-1)_h$ that produce γ_i and relative amounts of each isotopologue of the daughter compound $(\gamma+1)_j$ that are produced. For chloroethenes, these matrices, discussed in section 3.2, are generally sparse due to only one Cl, and no C, being lost in each degradation step.

3. Software and model

3.1. COMPEST

COMPEST is written in *java*, making use of the COMSOL Multiphysics *java* API. The tool is constructed so as to be general, with user options controlled via simple text files. In performing parameter estimation and uncertainty analysis, PEST varies the values of user-selected input parameters, via COMPEST, in order to estimate the Jacobian matrix. COMPEST, in effect, functions as an inter-agent for PEST and COMSOL Multiphysics (Fig. 1).

Java is an object-oriented, platform-independent, compiled language. As such, the compiled COMPEST *class* file can be run on any computer that has a *java* environment installed. In addition to standard *java* utilities, COMPEST requires parts of the com.comsol.model package. This package must therefore be added to PATH variables in the operating system or referenced explicitly when invoking *java*. Extensive instructions are included in the code repository.

Any model built in COMSOL Multiphysics can be used with COMPEST and PEST. Any values to be varied by PEST (e.g., for estimation or sensitivity analysis) must be defined as "variables" (as opposed to "parameters") during model preparation and should be deleted in the final .mph file called by COMPEST. The set-up of PEST input files, including the PEST control file (.pst extension), is the same as for any PEST application (Doherty, 2016a). Any number of observations or variables can be used when invoking COMPEST, although model outputs corresponding to the observations should be set up in COMSOL prior to execution. COMPEST exports these model outputs to .dat files (Fig. 1) which are then interpreted according to .ins files.

3.2. Model of groundwater contaminants

For the models considered in this paper, we consider isotopologues of PCE, TCE, and *c*DCE. While other decay sequences including *trans*-DCE are possible, in practice the decay sequence PCE→TCE→*c*DCE→VC (vinyl chloride) dominates (Fig. 2b). We consider the upper 1 m of an aquitard overlain by an aquifer (Fig. 3). In all cases considered here, diffusive flow is assumed to dominate in the aquitard and thus advective flow is negligible. The initial $\delta^{37}Cl$ and $\delta^{13}C$ values of present contaminants are, in effect, set to ~0 by defining the concentrations of each isotopologue according to $[\delta^{37}Cl/\delta^{35}Cl]_{\text{SMOC}} = 0.319766$ and

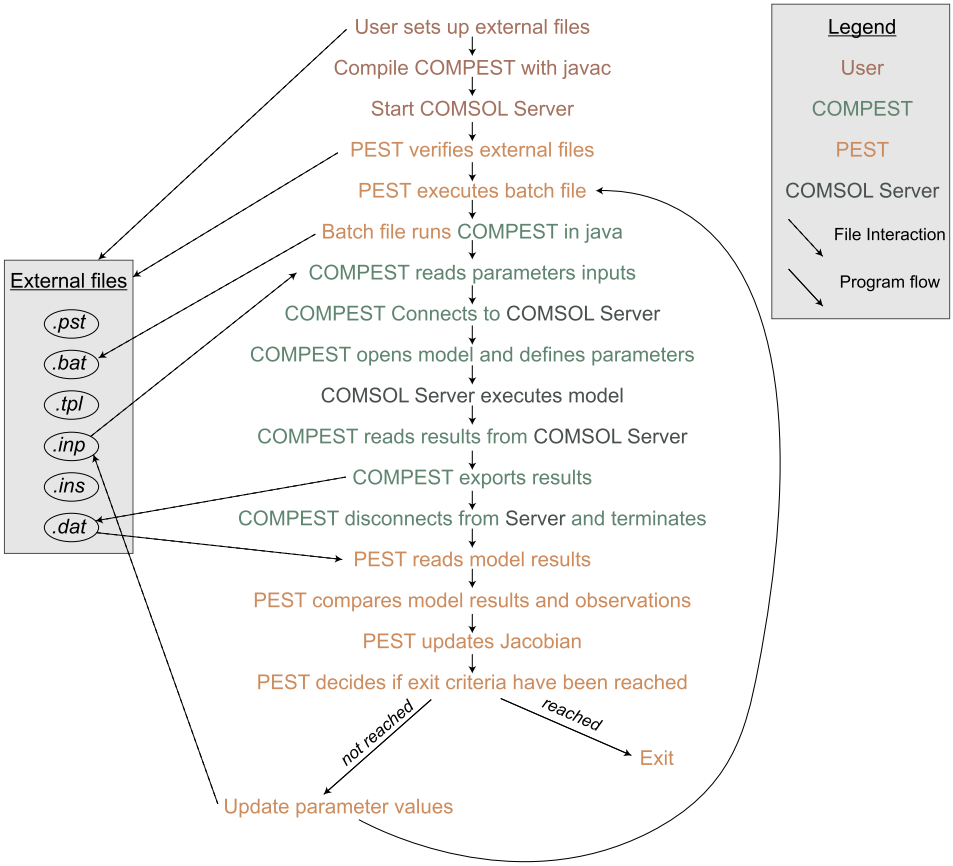

Fig. 1. Program flow showing interaction between COMPEST, COMSOL Multiphysics, PEST and external files. For simplicity, multiple files written by PEST are not shown here (see Doherty, 2016a). More detail on the procedure is available in the software repository.

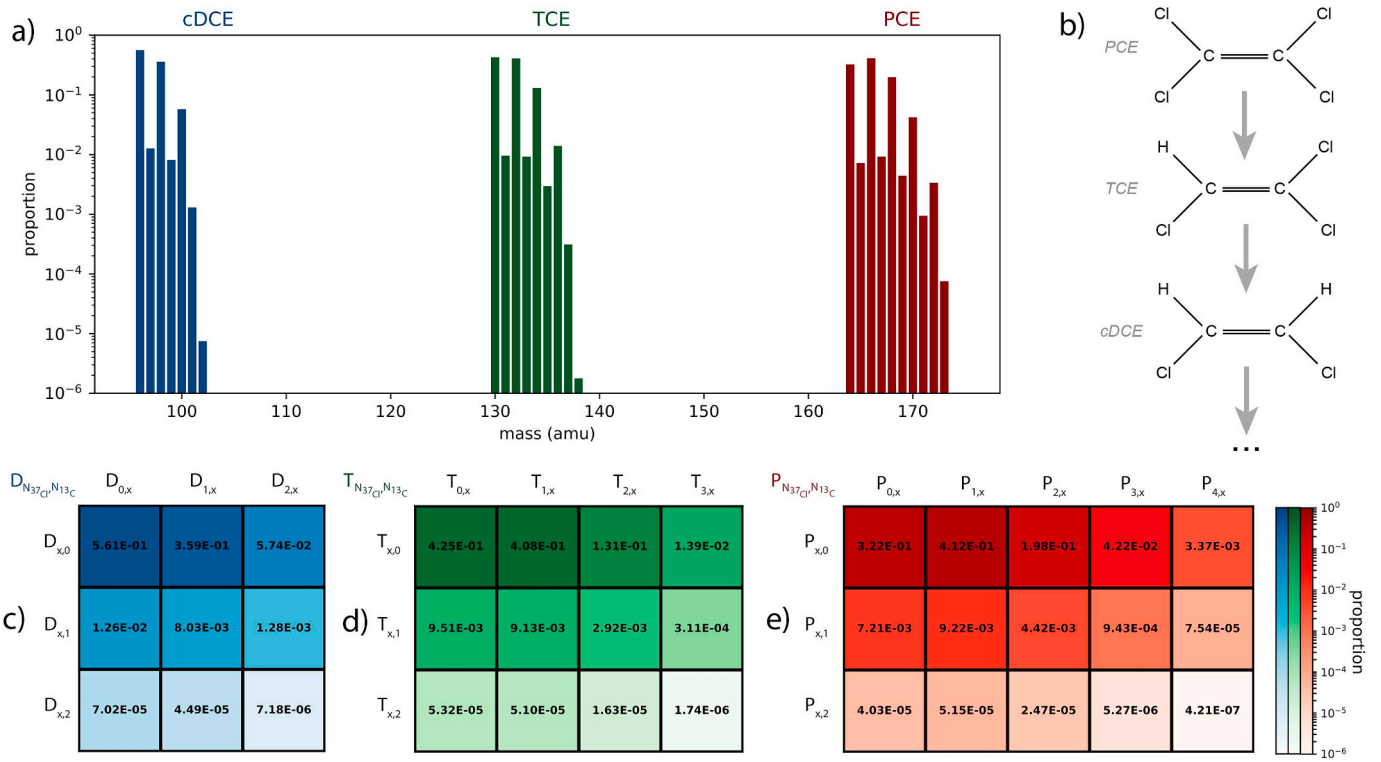

Fig. 2. *a)* Relative mass distributions for *c*DCE, TCE, and PCE at $\delta^{37}Cl \approx 0‰$ (relative to SMOC) and $\delta^{13}C \approx 0‰$ (relative to VPDB). *b)* PCE, TCE and *c*DCE molecules. The corresponding relative distributions of isotopologues for *c) c*DCE, *d)* TCE, and *e)* PCE. In *c), d),* and *e)* the columns correspond to different numbers of ^{37}Cl atoms and the rows to different numbers of ^{13}C atoms.

$[\delta^{13}C/\delta^{12}C]_{\mathrm{VPDB}} = 0.0111802$ (Fig. 2).

Two mechanisms for isotopic fractionation are implemented in the models: diffusion and degradation. The fluid diffusion coefficients, D, for each isotopologue are defined in relation to that of the average mass for the compound according to Equation (14). For PCE, the diffusion constants differed from the average by between −0.227% (PCE with 4 ^{37}Cl and 2 ^{13}C) and +0.059% (PCE with 0 ^{37}Cl and 0 ^{13}C). Similarly, isotopologue diffusion constants differed from the average by between −0.270% (TCE with 3 ^{37}Cl and 2 ^{13}C) and +0.042% (TCE with 0 ^{37}Cl and 0 ^{13}C) for TCE and by between −0.401% (*c*DCE with 2 ^{37}Cl and 2 ^{13}C) and +0.084% (*c*DCE with 0 ^{37}Cl and 0 ^{13}C) for *c*DCE. Hydrogen isotopes were not considered in the model.

The implemented isotope model (Equation (21)) is a modified version of the Badin et al. (2018) General Model. By considering isotopologues rather than isotopocules, we reduce the number of subspecies to be modelled for a given compound from $2^{N_C}2^{N_{Cl}}$ to $(N_C + 1)(N_{Cl} + 1)$, where N_C and N_{Cl} designate the number of C and Cl atoms, respectively. This reduction (from 64 to 15 species for PCE, for example) is due to the insensitivity to isotope position in the definition of an isotopologue. This, in effect, averages the secondary isotope effect (where a heavy isotope is in a non-reacting position) for all isotopologues. Badin et al. (2018) showed that an isotopocule-level model would only be needed in the hypothetical case of significantly contrasting position-specific secondary isotope effects, a phenomenon that, to date, has not been experimentally observed.

The model relies on transition matrices $\boldsymbol{\kappa}$ where the reaction rate of a given isotopologue depends on AKIE's: $A_{C,p}$ (C, primary), $A_{C,s}$ (C, secondary), $A_{Cl,p}$ (Cl, primary), and $A_{Cl,s}$ (Cl, secondary). Using the nomenclature $P_{N_{37_{Cl}},N_{13_C}}$, $T_{N_{37_{Cl}},N_{13_C}}$ and $D_{N_{37_{Cl}},N_{13_C}}$, where P refers to PCE, T refers to TCE, and D refers to *c*DCE, we calculate the transition matrices by reducing the position-sensitive portion of the Badin et al. (2018) general model. In these $\boldsymbol{\kappa}$ matrices (Tables A1–A3), we see that for parent isotopologues where $N_{Cl} = 0$, only one non-zero matrix element exists. This reflects the fact that only one daughter isotopologue is possible as there are no ^{37}Cl atoms to be lost during dechlorination. Similarly, where $N_{37_{Cl}} = N_{Cl}$ (i.e., all Chlorine atoms present are ^{37}Cl), there is only one non-zero row element as there are no ^{35}Cl atoms to be lost. For all other isotopologues, there are two non-zero row elements due to the possibility that either a ^{35}Cl or ^{37}Cl atom can be lost.

In the final example, explicit spatial and temporal variations in reaction rates are implemented. Depth-dependent reaction rates are implemented via a function $f_z(z)$ (Table 1) and time-dependent reaction rates via a function f_t. Following Van Breukelen et al. (2017) and Badin et al. (2018), optional Monod Kinetics (Kompala et al., 1984) are also implemented using the equation for each isotopologue γ_i of compound γ:

$$f_t = f_{\mathrm{Monod}}(B, C_{\gamma_i}) = \mu_{\gamma,\mathrm{Max}} \frac{BC_{\gamma_i}}{C_{\gamma_i} + K_{m,\gamma}} \tag{22}$$

where B is the biomass concentration consuming γ_i and $\mu_{\gamma,\mathrm{Max}}$ the maximum reaction rate per unit of B. If a stable bacterial population is assumed, this equation can be simplified (Bekins et al., 1998; Van Breukelen et al., 2017):

$$f_t = f_{\mathrm{Monod}}(C_{\gamma_i}) = R_\gamma \frac{C_{\gamma_i}}{C_{\gamma_i} + K_{m,\gamma}} \tag{23}$$

where R_γ is an reaction rate constant for compound γ. These functions are implemented as multipliers to Equation (21) and R is integrated into the f_t terms so that the reaction rate for a given isotopologue γ_i of compound γ is defined as:

$$\frac{\partial C_{\gamma_i}}{\partial t} = f_z(z)\left[f_{t,\gamma-1}\left[\sum_{h\in(\gamma-1)_{\mathrm{iso}}} \boldsymbol{\kappa}_{\gamma_h,\gamma_i}^{\gamma-1\to\gamma} \frac{C_{(\gamma-1)_h}}{C_{(\gamma-1)}}\right] - f_{t,\gamma}\left[\sum_{j\in(\gamma+1)_{\mathrm{iso}}} \boldsymbol{\kappa}_{\gamma_i,\gamma_j}^{\gamma\to\gamma+1}\right]\frac{C_{\gamma_i}}{C_\gamma}\right] \tag{24}$$

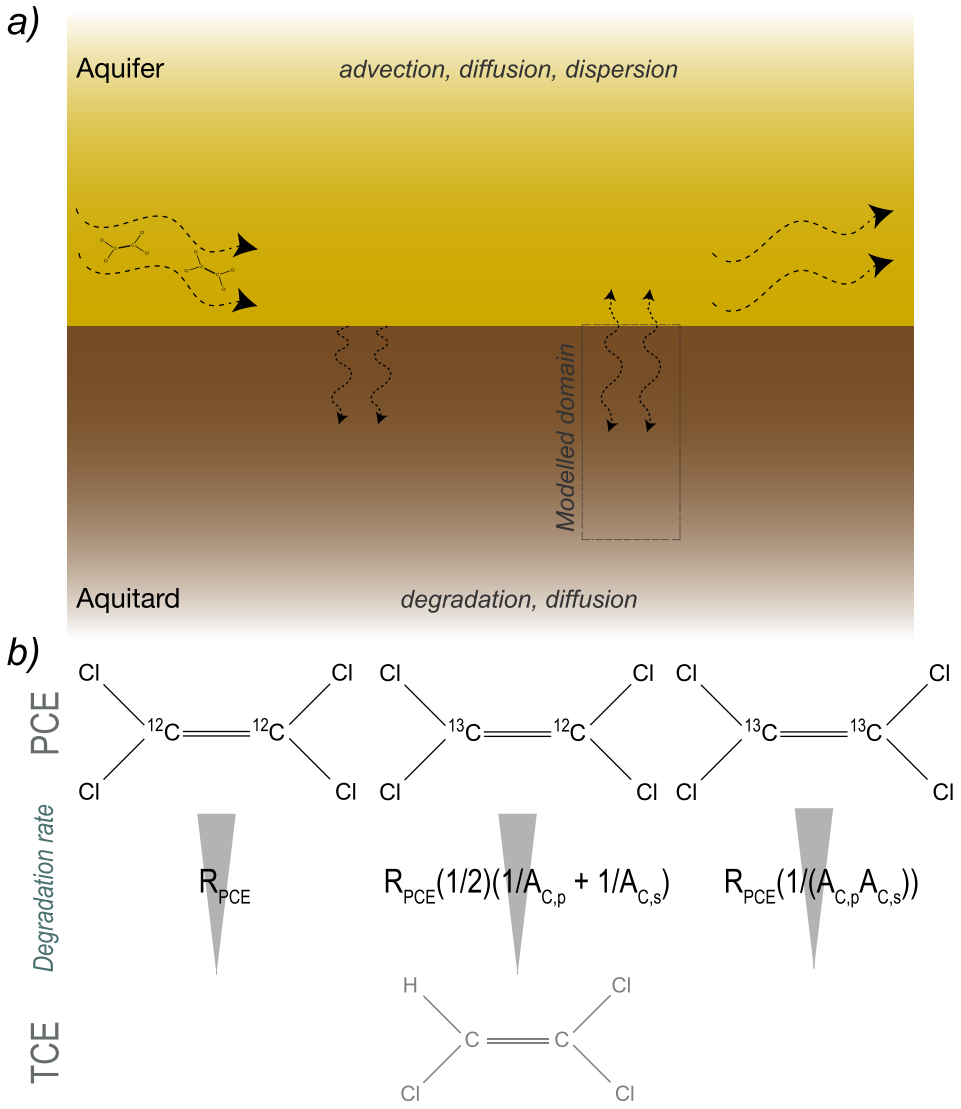

Fig. 3. *a)* Schematic showing the general process of diffusion into an aquitard (low permeability unit) and subsequent back-diffusion to the aquifer. The example models consider the aquitard and the upper domain boundary is the aquifer-aquitard interface. *b)* Schematic showing a simplified version (only C isotopes) of the degradation process that leads to isotopic enrichment and depletion. Here, the rate of degradation of each of the displayed isotopologues of PCE depends on the primary and secondary AKIEs of carbon ($A_{C,p}$ & $A_{C,s}$) which leads to isotopic enrichment of the parent compound. For simplicity, isotopologues of TCE are not shown.

In the examples presented here, Neumann-type boundary conditions were defined as:

$$D_{\gamma_i} \frac{\partial C_{\gamma_i}}{\partial z} = 0 \tag{25}$$

for each isotopologue γ_i.

4. Applications

Three examples of different COMPEST applications using versions of the model detailed in Section 3.2 are presented here. A heat-transport example is included in the Supplementary Information file to demonstrate how COMPEST can be used for other, unrelated applications.

4.1. Example 1: single-parameter, single-species model

To demonstrate COMPEST and the set-up procedure of the necessary files, we first consider a simple implementation of the model discussed in Section 3.2. We generate test observations of concentration and $\delta^{13}C$ data for PCE with selected parameters (Table 1). These data are generated for t= 0, 5, & 10 years, and for depths of 20 and 50 cm below the aquifer-aquitard interface. The total number of observations provided to PEST is thus twelve: six PCE concentration measurements and six PCE $\delta^{13}C$ measurements using CSIA. In practice, this type of dataset could be obtained over three sampling campaigns at two depths at the same location.

The f_t function is defined as a constant, R_{PCE} = 0.1 yr^{-1}, for PCE. We employ the procedure outlined in Fig. 1 to estimate a single unknown parameter, R_{PCE}. Weights for the two observation types are adjusted using the PEST utility program PWTADJ1 (Doherty, 2016b) to ensure that both $\delta^{13}C$ and C_{PCE} contribute significantly to the objective function. PEST is given an initial value of R_{PCE}= 0.001 yr^{-1}, with bounds of [10^{-5}, 10^{2}] yr^{-1}, and the parameter is log-transformed internally. While the underlying model for isotope fractionation is relatively complex, estimating a single parameter for a well-constrained application is straight-forward and requires only 29 model runs to determine the parameter exactly (i.e., R_{PCE}= 0.1000 yr^{-1}). By applying weights of zero to the concentration data or to the $\delta^{13}C$, basic insight into the utility of the concentration data and CSIA data in constraining the model can be gained. In the given configuration, when only $\delta^{13}C$ data is used, PEST requires 32 model runs, while when only C_{PCE} data is used, 29 model runs are required. This example illustrates the procedure in

Table 1
Values of parameters used in the examples presented in Section 4. Realistic D, K_m, & R values for chlorinated ethenes in clay aquitards were sourced from Badin et al. (2018). Examples 1, 2 and 3 are presented in Sections 4.1, 4.2 and 4.3, respectively. n/a = not applicable.

Variable	Example 1	Example 2	Example 3
D_{PCE}	9.4E-10 m^2/s	9.4E-10 m^2/s	9.4E-10 m^2/s
D_{TCE}	n/a	1.01E-9 m^2/s	1.01E-9 m^2/s
D_{cDCE}	n/a	1.13E-9 m^2/s	1.13E-9 m^2/s
$C_{PCE}(t=0)$	1 mol/m^3 $\in[-.1m,0m]$, 0 else	1 mol/m^3 $\in[-.1m,0m]$, 0 else	1 mol/m^3 $\in[-.1m,0m]$, 0 else
$C_{TCE}(t=0)$	n/a	0	0
$C_{cDCE}(t=0)$	n/a	0	0
$K_{m,PCE}$	n/a	n/a	0.0588 mol/m^3
$K_{m,TCE}$	n/a	n/a	0.0699 mol/m^3
$K_{m,cDCE}$	n/a	n/a	0.100 mol/m^3
$A_{C,p}$	1.02	1.02	1.02
$A_{Cl,p}$	n/a	1.005	1.005
$A_{C,s}$	1.000	1.001	1.001
$A_{Cl,s}$	n/a	1.0005	1.0005
R_{PCE}	0.1/yr	0.1/yr	0.1/yr
R_{TCE}	n/a	0.0685/yr	0.0685/yr
R_{cDCE}	n/a	0.0446/yr	0.0446/yr
f_z	1	1	Equation (26)
z_0	n/a	n/a	2 m

linking PEST and COMSOL Multiphysics using COMPEST and is recommended as a point of introduction for readers seeking to use the software.

4.2. Example 2: multi-parameter, multi-species model

The second example uses the same isotopic modelling approach outlined in Section 3.2 with most of the parameter values (Table 1) identical to those in the example of Section 4.1. As in the previous example, observation data is generated for two depths (20 and 50 cm) and three times (0, 5, & 10 years). However, here we make use of the concentration, $\delta^{13}C$, and $\delta^{37}Cl$ values for PCE, TCE and *c*DCE, resulting in 54 observation data points. To increase the complexity of the parameter estimation task, we attempt to estimate the values of 10 parameters: $A_{Cl,p}$, $A_{Cl,p}$, $A_{Cl,p}$, & $A_{Cl,p}$ (AKIEs); D_{PCE}, D_{TCE}, & D_{cDCE} (diffusion coefficients); and R_{PCE}, R_{TCE}, & R_{cDCE} (compound degradation rate constants). All but the AKIEs are log-transformed in PEST for parameter estimation. The primary AKIEs are limited to the theoretical range defined by the Streitwieser limit (Elsner et al., 2005) ($A_{Cl,p} \in [1,1.013]$; $A_{C,p} \in [1,1.057]$) while the secondary AKIEs are given a slightly more restrictive range ($A_{Cl,p} \in [1,1.0065]$; $A_{C,s} \in [1,1.0285]$). Each is given an initial value of 1. Diffusion coefficients are given initial values of 10^{-9} m^2/s and restricted to the range $[10^{-12},10^{-7}]$ m^2/s, while R_{PCE}, R_{TCE}, and R_{cDCE} are given initial values of 10^{-3} yr^{-1} and restricted to the range $[10^{-5},10^{2}]$ yr^{-1}.

In Example 1 (Section 4.1), the Jacobian matrix (Equation (8)) was size 12 × 1; here, it is 54 × 10 due to the increased number observations and parameters. As $m > n$, the problem may still be well-posed, but requires a higher number of model executions. During execution of the procedure outlined in Figure 1 and 19 optimization iterations were undertaken, resulting in 413 total model executions. Eight of the parameters were estimated exactly, while $A_{C,p}$ and $A_{C,s}$ were both estimated to be equal to 1.01041. Sensitivity analysis reveals that these two parameters the largest contributors to the objective function after parameter optimization (Fig. 4).

4.3. Example 3: variable reaction kinetics and SVD

In the final example, we introduce depth-dependent reaction rates and Monod kinetics, resulting in a significantly more complex model. We use this example to demonstrate the use of SVD in reducing the number of model runs required and in evaluating the eigenvectors of the solution space and the identifiabilities (Equation (11)) of the parameters.

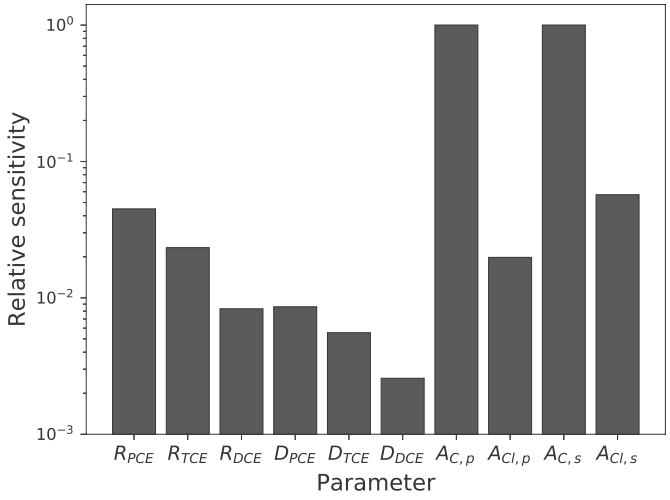

Fig. 4. Relative sensitivities of the objective function to the parameters in Example 2 at final estimated parameter values. $A_{C,p}$ and $A_{C,p}$ were the only parameters whose estimated values differed from their true values.

Depth-dependent reaction rates of the form

$$f_z(z) = 1 - \mathrm{erf}\left(\left|\frac{z}{z_0}\right|\right) = 1 - \frac{2}{\sqrt{\pi}}\int_0^{\left|\frac{z}{z_0}\right|} e^{-\zeta^2} d\zeta \tag{26}$$

have been proposed as an appropriate model to explain observed contaminant concentration profiles in low-permeability units (Wanner et al., 2016, 2018). This form has been implemented in Equation (24) with z_0 as a variable parameter. Following Van Breukelen et al. (2017) and Badin et al. (2018), Monod Kinetics (Equation (23)) were also implemented in the equation with differing values for R and K_m for each compound (Table 1). As with the other examples, at $t = 0$ there is a 1 mol/m^3 concentration of PCE (Table 1) in the upper 10 cm of the aquitard.

In the full model output, the dynamics of the degradation sequence and diffusion process can be clearly observed (Fig. 5). At the aquitard-aquifer boundary, the concentrations reach higher values and this occurs sooner than at deeper locations. The shifts in $\delta^{13}C$ and $\delta^{37}Cl$ are slightly more pronounced at deeper locations. Both of these behaviours are manifestations of the higher concentrations of PCE at shallow depths. PCE takes time to diffuse deeper into the aquitard and, during this time, is partially degraded to TCE and, subsequently, *c*DCE. During degradation, isotope shifts occur to a degree governed by the AKIEs. At early times, the isotope shifts of *c*DCE in particular are highly pronounced due to the exceedingly small amount of the compound, which requires two degradation steps to be produced, present.

The procedure of Fig. 1 is carried out with SVD restricted to a maximum of six singular values (eigenvalues). A total of 14 parameters (Fig. 6) are set as unknowns to be optimized. These include those of Section 4.2 as well as z_0 (Equation (26)) and the K_m values 23). As PEST is run in SVD mode and restricted to using only six linear combinations of the 14 parameters in the model, no parameters are estimated exactly (Table 2). However, the number of model runs executed is 189, less than half of those required in the simpler modelling case of Section 4.2.

5. Discussion

The PEST-COMPEST-COMSOL set-up is a powerful tool for estimating parameters and for understanding sensitivities and uncertainty in a forward model. The investigated phenomenon of isotope fractionation arises due to two processes, degradation and diffusion. The

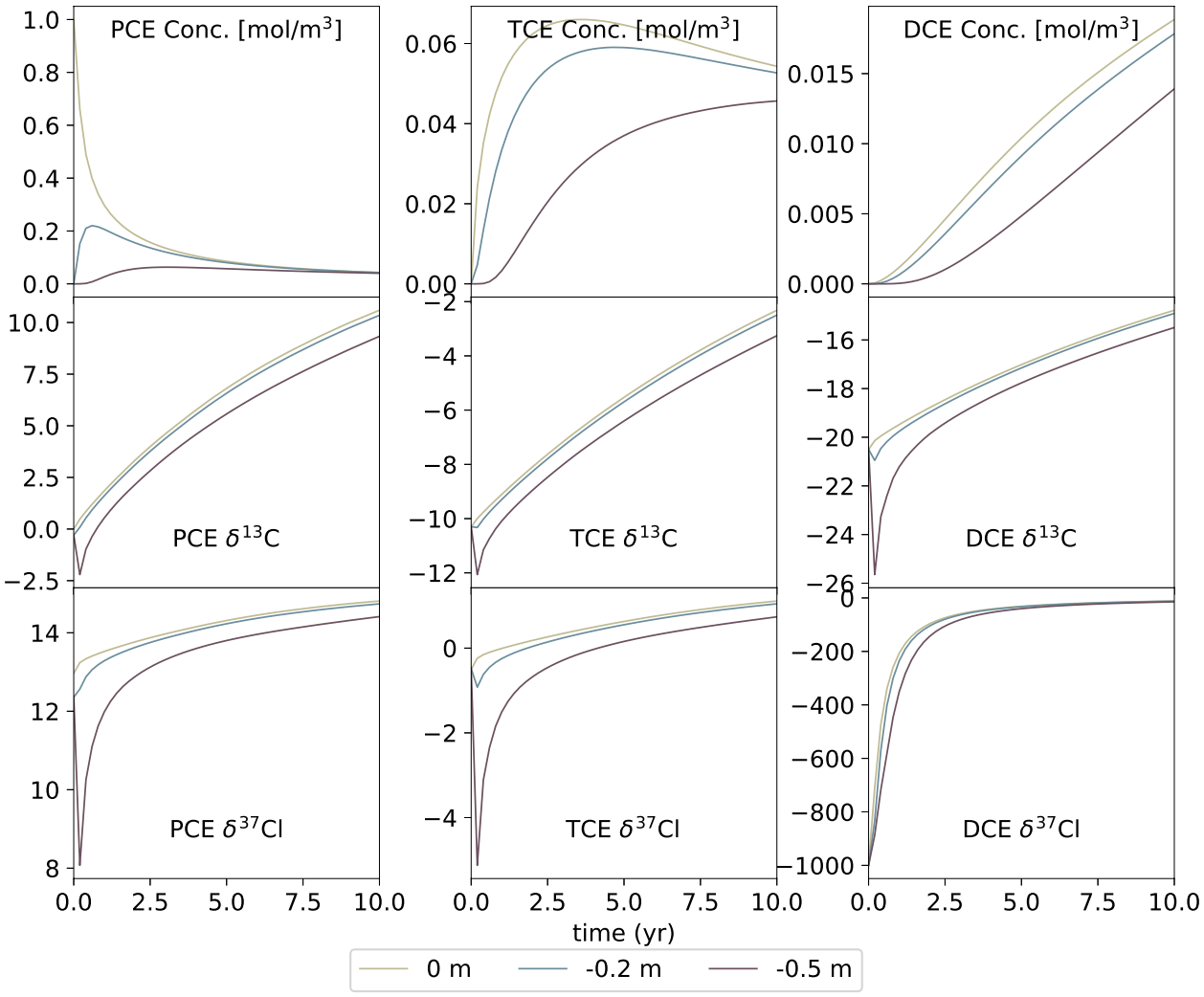

Fig. 5. Model output for three depths in the model Example 3, where Monod kinetics and depth-dependent reaction rates are implemented.

interplay between these two processes governs the temporal and spatial distribution of parent and daughter contaminant compounds in aquitards. This type of problem is a prime example of those to which the demonstrated method is well-suited.

The first example (Section 4.1) demonstrated a simple treatment of the inverse problem using the forward finite-element model. The complete fractionation framework using Equations (13), (14) and (24) is implemented, but only one parameter, R_{PCE}, is defined as an unknown. With one parameter and two types of observations, the input files (Fig. 1) are relatively simple, and should provide a point of entry for users. In the example, exact determination of the parameter was obtained with PCE concentration and PCE $\delta^{13}C$ observations, both combined and individually.

Example 2 (Section 4.2) uses the same model with simple reaction kinetics, but introduces additional parameters and observation types including those of daughter compounds TCE and cDCE. PEST was run in parameter estimation mode and SVD was not invoked, resulting in all parameters except the carbon AKIEs $A_{C,p}$ and $A_{C,s}$ being determined exactly. This result suggests that it may not be able to determine these parameters independently without restrictive parameter range assumptions. Closer inspection of the κ matrices (Tables A1-A3) reveals that $A_{C,p}$ and $A_{C,s}$ are never present independently. The terms appear as $1/A_{C,p} + 1/A_{C,s}$ and $1/(A_{C,p}A_{C,s})$ in many of the values. This reflects the fact that we consider only isotopologue-level effects (i.e., insensitive to the relative positions of individual atoms) in the model (Equation (21)) and that carbon atoms are never lost during degradation. The primary C AKIE is more pronounced and reflects the isotopic effect on reaction kinetics when a ^{13}C atom is present in a reacting position. Likewise, the secondary C AKIE describes the effect of a ^{13}C atom in a non-reacting position. As CSIA measures the mass distribution of a specific compound (and thus the isotopic enrichment values) and not the exact distribution of isotopes at each position in the compound, there would be no advantage in using a more complex isotopocule-level model. The insight into parameter interdependencies and sensitivities in this example illustrates the type of understanding that can be gained though the presented inverse modelling approach.

Finally, the third example (Section 4.3), wherein the majority of model parameters are allowed to vary, illustrates the utility of SVD in evaluating parameter identifiability and sensitivity. In the finite-element model, spatially-dependent reaction rates and Monod kinetics are introduced. The inclusion of these in models of contaminant degradation in low-permeability units has been discussed by Wanner et al. (2016), Van Breukelen et al. (2017) and Badin et al. (2018). The singular values of SVD span a large range (Fig. 6b). This suggests that acceptable model performance in predicting the evolution of contaminant concentration and isotopic enrichment (i.e., the same types of observations that the model is calibrated against) can be obtained by using a smaller number of "superparameters" or eigenvectors. These eigenvectors are linear combinations of the model parameters and, together, span the solution space. The degree to which the solution space is spanned by using fewer eigenvectors than parameters (here, six eigenvectors for 14 parameters) is shown by the identifiabilities (Fig. 6c)

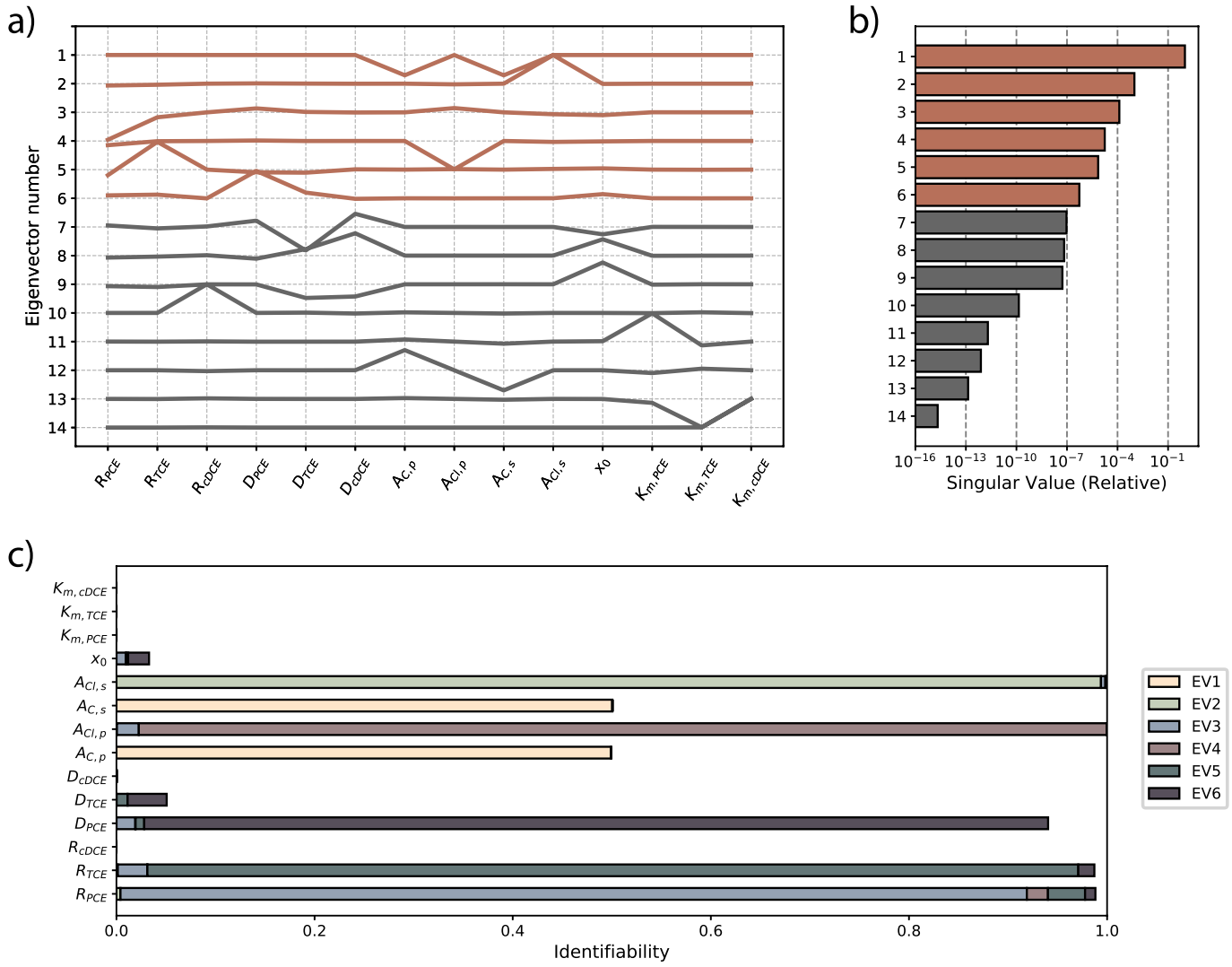

Fig. 6. Details of SVD with six eigenvectors in Example 3: *a)* eigenvectors (values ranging between −1 & 1) and their corresponding *b)* singular values (eigenvalues). *c)* Identifiabilities (Equation (11)) of the parameters and the corresponding contribution of the six eigenvectors ('EV1' – 'EV6') with the greatest singular values.

Table 2
Parameter estimates and their error with respect to the true parameter values (Table 1) for a six-parameter SVD run. †*For AKIEs, error is calculated for the estimate of* $(A - 1)$.

Parameter	Estimated Value	Error	Identifiability (ξ)
R_{PCE}	8.3707E-02	−16%	9.882E-01
R_{TCE}	5.8057E-02	−15%	9.872E-01
R_{cDCE}	9.9942E-04	−98%	1.064E-05
D_{PCE}	7.9926E-10	−15%	9.404E-01
D_{TCE}	7.2967E-10	−28%	5.074E-02
D_{cDCE}	5.0561E-10	−55%	4.896E-04
$A_{C,p}$	1.0107E+00	−46%†	4.993E-01
$A_{Cl,p}$	1.0035E+00	−30%†	1.000E+00
$A_{C,s}$	1.0100E+00	899%†	5.007E-01
$A_{Cl,s}$	1.0013E+00	159%†	1.000E+00
z_0	3.2473E+00	62%	3.292E-02
$K_{m,PCE}$	4.9997E+01	−15%	1.321E-05
$K_{m,TCE}$	4.9988E+01	−28%	1.839E-05
$K_{m,cDCE}$	5.0000E+01	−50%	4.086E-10

which gives an indication of the effect of individual parameters on model output and, consequently, the ability of PEST to constrain them. Parameters with larger errors using the truncated SVD (Table 2) generally correspond to those with the lower identifiabilities.

In the presented examples, the models could be executed relatively rapidly (< 15 s on Intel i7 2.8 GHz PC with 16 GB RAM), which posed little issue in using COMSOL to solve the inverse problem. For larger models (e.g., those with a large number of nodes and/or highly non-linear behaviour), users may wish to investigate running COMPEST with BeoPEST (Schreuder, 2009) or PEST++ (Welter et al., 2015) and using multiple COMSOL Multiphysics servers running in parallel.

6. Conclusions and outlook

Using forward finite element models as tools to solve inverse problems can be a powerful approach. COMSOL Multiphysics allows for a high degree of model versatility and can couple multiple processes. Although it is not a likely candidate to supplant distributed hydrological models such as SWAT (Arnold et al., 2012) or Hydrogeosphere (Brunner et al., 2009) for catchment hydrology applications, its adaptability to specific problems makes it appealing for various applications in the geosciences (e.g., Butler and Sinha, 2012; Jin et al., 2014; Zhou et al., 2014; Lippmann-Pipke et al., 2017). In any inverse modelling application, parameter estimates are more valuable in making assessments if there is an understanding of the modelling approach's ability to determine the true values of these parameters. PEST, used in conjunction with COMPEST and COMSOL Multiphysics, can be used to provide this type of insight.

Geoscientists investigating problems where multiple physical, geochemical, and other processes interact often need models to constrain parameters that cannot be directly measured. We have demonstrated how COMPEST facilitates this by performing inverse modelling using forward finite-element models. The case of isotopic fractionation of groundwater contaminants due to degradation and diffusion is exemplary of the style of problem for which we expect COMPEST to be useful. It is our hope that geoscientists who require parameter estimates and uncertainty analysis find the presented code and demonstrations useful. Likewise, we also encourage those using finite-element models to address inverse problems in domains outside of geoscience to explore the method outlined here.

Code availability

- Name of code: COMPEST
- Developer and contact info: Dr. Landon J.S. Halloran (landon.halloran@unine.ch, +41 327182649, www.ljsh.ca), Centre d'hydrogéologie et de géothermie, Université de Neuchâtel, rue Émile-Argand 11, 2000 Neuchâtel, Suisse.
- Year first available: 2019
- Hardware required: Windows PC (tested with Windows 10)
- Software required: COMSOL Multiphysics Server (tested with ver. 5.3) and COMSOL Java API, Java IDE (tested with ver. 1.8), PEST (ver. 12.1.0 executable included with COMPEST).
- Program language: Java
- Program size: ~44 MB (all files, including examples); < 20 KB (COMPEST source code and class, not including dependences and input files)
- How to access the source code: COMPEST, all associated files, a detailed README and all examples presented in this article are available at: https://github.com/lhalloran/COMPEST or https://doi.org/10.5281/zenodo.2553569.

Authorship statement

LJSH conceived the paper & software, wrote the code & manuscript, and created & validated the examples. PB assisted with project supervision, provided PEST advice, and provided feedback to improve the manuscript. DH supervised and secured funding for the project, provided advice on isotopes and contaminants, and provided feedback to improve the manuscript.

Acknowledgements

LJSH and DH received funding from the Swiss National Science Foundation (FNS/SNF) Project "Tracking reactive processes in low permeability sediments and their effect on contaminant longevity in aquifers using compound-specific isotope analysis," [Grant number: 166233] (http://p3.snf.ch/Project-166233). We acknowledge the python library *matplotlib* (Hunter, 2007) which was used to create some of the figures (source code of which is available in the COMPEST repository). We would also like to thank Editor Dario Grana, Associate Editor Ute Mueller, and the three reviewers for their encouraging feedback.

Appendix A. Supplementary data

Supplementary data to this article can be found online at https://doi.org/10.1016/j.cageo.2019.02.001.

Appendices

Table A1
Transition matrix $\kappa^{\mathrm{PCE}\rightarrow\mathrm{TCE}}$ for the decay of PCE to TCE

	$\boldsymbol{T}_{0,0}$	$\boldsymbol{T}_{0,1}$	$\boldsymbol{T}_{0,2}$	$\boldsymbol{T}_{1,0}$	$\boldsymbol{T}_{1,1}$	$\boldsymbol{T}_{1,2}$
$\boldsymbol{P}_{0,0}$	1	0	0	0	0	0
$\boldsymbol{P}_{0,1}$	0	$\frac{1}{2}\left(\frac{1}{A_{C,p}}+\frac{1}{A_{C,s}}\right)$	0	0	0	0
$\boldsymbol{P}_{0,2}$	0	0	$\frac{1}{A_{C,p}}\frac{1}{A_{C,s}}$	0	0	0
$\boldsymbol{P}_{1,0}$	$\frac{1}{4}\frac{1}{A_{Cl,p}}$	0	0	$\frac{3}{4}\frac{1}{A_{Cl,s}}$	0	0
$\boldsymbol{P}_{1,1}$	0	$\left(\frac{1}{8}\frac{1}{A_{Cl,p}}\right)\left(\frac{1}{A_{C,p}}+\frac{1}{A_{C,s}}\right)$	0	0	$\left(\frac{3}{8}\frac{1}{A_{Cl,s}}\right)\left(\frac{1}{A_{C,p}}+\frac{1}{A_{C,s}}\right)$	0
$\boldsymbol{P}_{1,2}$	0	0	$\frac{1}{4}\frac{1}{A_{Cl,p}}\frac{1}{A_{C,p}A_{C,s}}$	0	0	$\frac{3}{4}\frac{1}{A_{Cl,s}}\frac{1}{A_{C,p}A_{C,s}}$
$\boldsymbol{P}_{2,0}$	0	0	0	$\frac{1}{2}\frac{1}{A_{Cl,p}A_{Cl,s}}$	0	0
$\boldsymbol{P}_{2,1}$	0	0	0	0	$\frac{1}{4}\frac{1}{A_{Cl,p}A_{Cl,s}}\left(\frac{1}{A_{C,p}}+\frac{1}{A_{C,s}}\right)$	0
$\boldsymbol{P}_{2,2}$	0	0	0	0	0	$\frac{1}{2}\frac{1}{A_{Cl,p}A_{Cl,s}}\frac{1}{A_{C,p}A_{C,s}}$
$\boldsymbol{P}_{3,0}$	0	0	0	0	0	0
$\boldsymbol{P}_{3,1}$	0	0	0	0	0	0
$\boldsymbol{P}_{3,2}$	0	0	0	0	0	0
$\boldsymbol{P}_{4,0}$	0	0	0	0	0	0
$\boldsymbol{P}_{4,1}$	0	0	0	0	0	0
$\boldsymbol{P}_{4,2}$	0	0	0	0	0	0

	$\boldsymbol{T}_{2,0}$	$\boldsymbol{T}_{2,1}$	$\boldsymbol{T}_{2,2}$	$\boldsymbol{T}_{3,0}$	$\boldsymbol{T}_{3,1}$	$\boldsymbol{T}_{3,2}$
$\boldsymbol{P}_{0,0}$	0	0	0	0	0	0
$\boldsymbol{P}_{0,1}$	0	0	0	0	0	0
$\boldsymbol{P}_{0,2}$	0	0	0	0	0	0
$\boldsymbol{P}_{1,0}$	0	0	0	0	0	0

(*continued on next page*)

Table A1 (*continued*)

	$\boldsymbol{T}_{0,0}$	$\boldsymbol{T}_{0,1}$	$\boldsymbol{T}_{0,2}$	$\boldsymbol{T}_{1,0}$	$\boldsymbol{T}_{1,1}$	$\boldsymbol{T}_{1,2}$
$\boldsymbol{P}_{1,1}$	0	0	0	0	0	0
$\boldsymbol{P}_{1,2}$	0	0	0	0	0	0
$\boldsymbol{P}_{2,0}$	$\frac{1}{2}\frac{1}{A_{Cl,s}^2}$	0	0	0	0	0
$\boldsymbol{P}_{2,1}$	0	$\frac{1}{4}\frac{1}{A_{Cl,s}^2}\left(\frac{1}{A_{C,p}}+\frac{1}{A_{C,s}}\right)$	0	0	0	0
$\boldsymbol{P}_{2,2}$	0	0	$\frac{1}{2}\frac{1}{A_{Cl,s}^2}\frac{1}{A_{C,p}A_{C,s}}$	0	0	0
$\boldsymbol{P}_{3,0}$	$\frac{3}{4}\frac{1}{A_{Cl,p}A_{Cl,s}^2}$	0	0	$\frac{1}{4}\frac{1}{A_{Cl,s}^3}$	0	0
$\boldsymbol{P}_{3,1}$	0	$\frac{3}{8}\frac{1}{A_{Cl,p}A_{Cl,s}^2}\left(\frac{1}{A_{C,p}}+\frac{1}{A_{C,s}}\right)$	0	0	$\frac{1}{8}\frac{1}{A_{Cl,s}^3}\left(\frac{1}{A_{C,p}}+\frac{1}{A_{C,s}}\right)$	0
$\boldsymbol{P}_{3,2}$	0	0	$\frac{3}{4}\frac{1}{A_{Cl,p}A_{Cl,s}^2}\frac{1}{A_{C,p}A_{C,s}}$	0	0	$\frac{1}{4}\frac{1}{A_{Cl,s}^3}\frac{1}{A_{C,p}A_{C,s}}$
$\boldsymbol{P}_{4,0}$	0	0	0	$\frac{1}{A_{Cl,p}A_{Cl,s}^3}$	0	0
$\boldsymbol{P}_{4,1}$	0	0	0	0	$\frac{1}{A_{Cl,p}A_{Cl,s}^3}\left(\frac{1}{A_{C,p}}+\frac{1}{A_{C,s}}\right)$	0
$\boldsymbol{P}_{4,2}$	0	0	0	0	0	$\frac{1}{A_{Cl,p}A_{Cl,s}^3}\frac{1}{A_{C,p}A_{C,s}}$

Table A2
Transition matrix $\kappa^{\mathrm{TCE}\rightarrow c\mathrm{DCE}}$ for the decay of TCE to *c*DCE

	$\boldsymbol{D}_{0,0}$	$\boldsymbol{D}_{0,1}$	$\boldsymbol{D}_{0,2}$	$\boldsymbol{D}_{1,0}$	$\boldsymbol{D}_{1,1}$
$\boldsymbol{T}_{0,0}$	1	0	0	0	0
$\boldsymbol{T}_{0,1}$	0	$\frac{1}{2}\frac{1}{A_{C,p}}+\frac{1}{2}\frac{1}{A_{C,s}}$	0	0	0
$\boldsymbol{T}_{0,2}$	0	0	$\frac{1}{A_{C,p}}\frac{1}{A_{C,s}}$	0	0
$\boldsymbol{T}_{1,0}$	$\frac{1}{3}\frac{1}{A_{Cl,p}}$	0	0	$\frac{2}{3}\frac{1}{A_{Cl,s}}$	0
$\boldsymbol{T}_{1,1}$	0	$\left(\frac{1}{6}\frac{1}{A_{Cl,p}}\right)\left(\frac{1}{A_{C,p}}+\frac{1}{A_{C,s}}\right)$	0	0	$\left(\frac{1}{3}\frac{1}{A_{Cl,s}}\right)\left(\frac{1}{A_{C,p}}+\frac{1}{A_{C,s}}\right)$
$\boldsymbol{T}_{1,2}$	0	0	$\frac{1}{3}\frac{1}{A_{Cl,p}}\frac{1}{A_{C,p}A_{C,s}}$	0	0
$\boldsymbol{T}_{2,0}$	0	0	0	$\frac{2}{3}\frac{1}{A_{Cl,p}A_{Cl,s}}$	0
$\boldsymbol{T}_{2,1}$	0	0	0	0	$\frac{1}{3}\frac{1}{A_{Cl,p}A_{Cl,s}}\left(\frac{1}{A_{C,p}}+\frac{1}{A_{C,s}}\right)$
$\boldsymbol{T}_{2,2}$	0	0	0	0	0
$\boldsymbol{T}_{3,0}$	0	0	0	0	0
$\boldsymbol{T}_{3,1}$	0	0	0	0	0
$\boldsymbol{T}_{3,2}$	0	0	0	0	0

	$\boldsymbol{D}_{1,2}$	$\boldsymbol{D}_{2,0}$	$\boldsymbol{D}_{2,1}$	$\boldsymbol{D}_{2,2}$
$\boldsymbol{T}_{0,0}$	0	0	0	0
$\boldsymbol{T}_{0,1}$	0	0	0	0
$\boldsymbol{T}_{0,2}$	0	0	0	0
$\boldsymbol{T}_{1,0}$	0	0	0	0
$\boldsymbol{T}_{1,1}$	0	0	0	0
$\boldsymbol{T}_{1,2}$	$\frac{2}{3}\frac{1}{A_{Cl,s}}\frac{1}{A_{C,p}A_{C,s}}$	0	0	0
$\boldsymbol{T}_{2,0}$	0	$\frac{1}{3}\frac{1}{A_{Cl,s}^2}$	0	0
$\boldsymbol{T}_{2,1}$	0	0	$\frac{1}{6}\frac{1}{A_{Cl,s}^2}\left(\frac{1}{A_{C,p}}+\frac{1}{A_{C,s}}\right)$	0
$\boldsymbol{T}_{2,2}$	$\frac{2}{3}\frac{1}{A_{Cl,p}A_{Cl,s}}\frac{1}{A_{C,p}A_{C,s}}$	0	0	$\frac{1}{3}\frac{1}{A_{Cl,s}^2}\frac{1}{A_{C,p}A_{C,s}}$
$\boldsymbol{T}_{3,0}$	0	$\frac{1}{A_{Cl,p}A_{Cl,s}^2}$	0	0
$\boldsymbol{T}_{3,1}$	0	0	$\frac{1}{A_{Cl,p}A_{Cl,s}^2}\left(\frac{1}{A_{C,p}}+\frac{1}{A_{C,s}}\right)$	0
$\boldsymbol{T}_{3,2}$	0	0	0	$\frac{1}{A_{Cl,p}A_{Cl,s}^2}\frac{1}{A_{C,p}A_{C,s}}$

Table A3
Transition matrix $\kappa^{cDCE \rightarrow VC}$ for the decay of *c*DCE to vinyl chloride

	$\boldsymbol{V}_{0,0}$	$\boldsymbol{V}_{0,1}$	$\boldsymbol{V}_{0,2}$	$\boldsymbol{V}_{1,0}$	$\boldsymbol{V}_{1,1}$	$\boldsymbol{V}_{1,2}$
$\boldsymbol{D}_{0,0}$	1	0	0	0	0	0
$\boldsymbol{D}_{0,1}$	0	$\frac{1}{2}\frac{1}{A_{C,p}} + \frac{1}{2}\frac{1}{A_{C,s}}$	0	0	0	0
$\boldsymbol{D}_{0,2}$	0	0	$\frac{1}{A_{C,p}}\frac{1}{A_{C,s}}$	0	0	0
$\boldsymbol{D}_{1,0}$	$\frac{1}{2}\frac{1}{A_{Cl,p}}$	0	0	$\frac{1}{2}\frac{1}{A_{Cl,s}}$	0	0
$\boldsymbol{D}_{1,1}$	0	$\left(\frac{1}{4}\frac{1}{A_{Cl,p}}\right)\left(\frac{1}{A_{C,p}} + \frac{1}{A_{C,s}}\right)$	0	0	$\left(\frac{1}{4}\frac{1}{A_{Cl,s}}\right)\left(\frac{1}{A_{C,p}} + \frac{1}{A_{C,s}}\right)$	0
$\boldsymbol{D}_{1,2}$	0	0	$\frac{1}{2}\frac{1}{A_{Cl,p}}\frac{1}{A_{C,p}}\frac{1}{A_{C,s}}$	0	0	$\frac{1}{2}\frac{1}{A_{Cl,s}}\frac{1}{A_{C,p}}\frac{1}{A_{C,s}}$
$\boldsymbol{D}_{2,0}$	0	0	0	$\frac{1}{A_{Cl,p}A_{Cl,s}}$	0	0
$\boldsymbol{D}_{2,1}$	0	0	0	0	$\frac{1}{2}\frac{1}{A_{Cl,p}A_{Cl,s}}\left(\frac{1}{A_{C,p}} + \frac{1}{A_{C,s}}\right)$	0
$\boldsymbol{D}_{2,2}$	0	0	0	0	0	$\frac{1}{A_{Cl,p}A_{Cl,s}}\frac{1}{A_{C,p}A_{C,s}}$

References

Adrian, L., Löffler, F.E., 2016. Organohalide-Respiring Bacteria. Springer.

Andrews, H., Patterson, C., 1976. Singular value decomposition (SVD) image coding. IEEE Trans. Commun. 24 (4), 425–432. https://doi.org/10.1109/TCOM.1976.1093309.

Arnold, J., Moriasi, D.N., Gassman, P.W., Abbaspour, K.C., White, M.J., Srinivasan, R., Santhi, C., Harmel, R.D., van Griensven, A., Van Liew, M.W., Kannan, N., Jha, M.K., 2012. SWAT: model use, calibration, and validation. Trans. ASABE 55 (4), 1491–1508. https://doi.org/10.13031/2013.42256.

Audí-Miró, C., Cretnik, S., Otero, N., Palau, J., Shouakar-Stash, O., Soler, A., Elsner, M., 2013. Cl and C isotope analysis to assess the effectiveness of chlorinated ethene degradation by zero-valent iron: evidence from dual element and product isotope values. Appl. Geochem. 32, 175–183. https://doi.org/10.1016/j.apgeochem.2012.08.025.

Azad, V.J., Li, C., Verba, C., Ideker, J.H., Isgor, O.B., 2016. A COMSOL–GEMS interface for modeling coupled reactive-transport geochemical processes. Comput. Geosci. 92, 79–89. https://doi.org/10.1016/j.cageo.2016.04.002.

Badin, A., Braun, F., Halloran, L.J.S., Maillard, J., Hunkeler, D., 2018. Modelling of C/Cl isotopic behaviour during chloroethene biotic reductive dechlorination: capabilities and limitations of simplified and comprehensive models. PLoS One 13 (8), e0202416. https://doi.org/10.1371/journal.pone.0202416.

Badin, A., Broholm, M.M., Jacobsen, C.S., Palau, J., Dennis, P., Hunkeler, D., 2016. Identification of abiotic and biotic reductive dechlorination in a chlorinated ethene plume after thermal source remediation by means of isotopic and molecular biology tools. J. Contam. Hydrol. 192, 1–19. https://doi.org/10.1016/j.jconhyd.2016.05.003.

Baginska, B., Milne-Home, W., Cornish, P., 2003. Modelling nutrient transport in currency creek, NSW with AnnAGNPS and PEST. Environ. Model. Softw 18 (8–9), 801–808. https://doi.org/10.1016/S1364-8152(03)00079-3.

Bahremand, A., De Smedt, F., 2008. Distributed hydrological modeling and sensitivity analysis in torysa watershed, Slovakia. Water Resour. Manag. 22 (3), 393–408. https://doi.org/10.1007/s11269-007-9168-x.

Bekins, B.A., Warren, E., Godsy, E.M., 1998. A comparison of zero-order, first-order, and Monod biotransformation models. Gr. Water 36 (2), 261–268. https://doi.org/10.1111/j.1745-6584.1998.tb01091.x.

Brunner, P., Cook, P.G., Simmons, C.T., 2009. Hydrogeologic controls on disconnection between surface water and groundwater. Water Resour. Res. 45 (W1422), 1–13. https://doi.org/10.1029/2008WR006953.

Butler, S., Sinha, G., 2012. Forward modeling of applied geophysics methods using Comsol and comparison with analytical and laboratory analog models. Comput. Geosci. 42, 168–176. https://doi.org/10.1016/j.cageo.2011.08.022.

Cardenas, M.B., 2007. Potential contribution of topography-driven regional groundwater flow to fractal stream chemistry: residence time distribution analysis of Tóth flow. Geophys. Res. Lett. 34 (5), 1–5. https://doi.org/10.1029/2006GL029126.

Chui, T.F.M., Freyberg, D.L., 2009. Implementing hydrologic boundary conditions in a multiphysics model. J. Hydrol. Eng. 14 (12), 1374–1377. https://doi.org/10.1061/(ASCE)HE.1943-5584.0000113.

Cincinelli, A., Pieri, F., Zhang, Y., Seed, M., Jones, K.C., 2012. Compound Specific Isotope Analysis (CSIA) for chlorine and bromine: a review of techniques and applications to elucidate environmental sources and processes. Environ. Pollut. 169, 112–127. https://doi.org/10.1016/j.envpol.2012.05.006.

COMSOL, 2014. COMSOL Multiphysics User's Guide, 5.0 edition. COMSOL AB.

Coplen, T.B., Brand, W.A., Gehre, M., Gröning, M., Meijer, H.A.J., Toman, B., Verkouteren, R.M., 2006. New guidelines for δ 13 C measurements. Anal. Chem. 78 (7), 2439–2441. https://doi.org/10.1021/ac052027c.

Crane, R., Scott, T., 2012. Nanoscale zero-valent iron: future prospects for an emerging water treatment technology. J. Hazard Mater. 211–212, 112–125. https://doi.org/10.1016/j.jhazmat.2011.11.073.

Cullen, M., Freitag, M.A., Kindermann, S., Scheichl, R. (Eds.), 2013. Large Scale Inverse Problems: Computational Methods and Applications in the Earth Sciences. De Gruyter, Berlin.

Doherty, J., 2015. Calibration and Uncertainty Analysis for Complex Environmental Models. Watermark Numerical Computing, Brisbane.

Doherty, J., 2016a. PEST Model-independent Parameter Estimation User Manual Part I: PEST, SENSAN and Global Optimisers, 6 edition. Watermark Numerical Computing, Brisbane.

Doherty, J., Hunt, R.J., 2009. Two statistics for evaluating parameter identifiability and error reduction. J. Hydrol. 366 (1–4), 119–127. https://doi.org/10.1016/j.jhydrol.2008.12.018.

Doherty, J.E., 2016b. PEST Model-independent Parameter Estimation User Manual Part II: PEST Utility Support Software, 6 edition. Watermark Numerical Computing, Brisbane.

Elsner, M., 2010. Stable isotope fractionation to investigate natural transformation mechanisms of organic contaminants: principles, prospects and limitations. J. Environ. Monit. 12 (11), 2005–2031. https://doi.org/10.1039/c0em00277a.

Elsner, M., Couloume, G.L., Mancini, S., Burns, L., Lollar, B.S., 2010. Carbon isotope analysis to evaluate nanoscale Fe(O) treatment at a chlorohydrocarbon contaminated site. Ground Water Monit. Remediation 30 (3), 79–95. https://doi.org/10.1111/j.1745-6592.2010.01294.x.

Elsner, M., Zwank, L., Hunkeler, D., Schwarzenbach, R.P., 2005. A new concept linking observable stable isotope fractionation to transformation pathways of organic pollutants. Environ. Sci. Technol. 39 (18), 6896–6916. https://doi.org/10.1021/es0504587.

Fjordboge, A.S., Lange, I.V., Bjerg, P.L., Binning, P.J., Riis, C., Kjeldsen, P., 2012. ZVI-Clay remediation of a chlorinated solvent source zone, Skuldelev, Denmark: 2. Groundwater contaminant mass discharge reduction. J. Contam. Hydrol. 140–141, 67–79. https://doi.org/10.1016/j.jconhyd.2012.08.009.

Gleeson, T., Befus, K.M., Jasechko, S., Luijendijk, E., Cardenas, M.B., 2015. The global volume and distribution of modern groundwater. Nat. Geosci. 9 (2), 161–167. https://doi.org/10.1038/ngeo2590.

Halloran, L.J., Andersen, M.S., Rau, G.C., 2017. Investigation of the thermal regime and subsurface properties of a tidally affected, variably saturated streambed. Hydrol. Process. 31 (14), 2541–2555. https://doi.org/10.1002/hyp.11197.

Hammarström, B., Evander, M., Barbeau, H., Bruzelius, M., Larsson, J., Laurell, T., Nilsson, J., 2010. Non-contact acoustic cell trapping in disposable glass capillaries. Lab Chip 10 (17), 2251. https://doi.org/10.1039/c004504g.

Heron, G., Bierschenk, J., Swift, R., Watson, R., Kominek, M., 2016. Thermal DNAPL source zone treatment impact on a CVOC plume. Groundw. Monit. Remediat. 36 (1), 26–37. https://doi.org/10.1111/gwmr.12148.

Hunkeler, D., Aravena, R., Berry-Spark, K., Cox, E., 2005. Assessment of degradation pathways in an aquifer with mixed chlorinated hydrocarbon contamination using stable isotope analysis. Environ. Sci. Technol. 39 (16), 5975–5981. https://doi.org/10.1021/es048464a.

Hunter, J.D., 2007. Matplotlib: a 2D graphics environment. Comput. Sci. Eng. 9 (3), 90–95. https://doi.org/10.1109/MCSE.2007.55.

Jin, Y., Holzbecher, E., Sauter, M., 2014. A novel modeling approach using arbitrary Lagrangian–Eulerian (ALE) method for the flow simulation in unconfined aquifers. Comput. Geosci. 62, 88–94. https://doi.org/10.1016/j.cageo.2013.10.002.

Keyes, D.E., McInnes, L.C., Woodward, C., Gropp, W., Myra, E., Pernice, M., Bell, J., Brown, J., Clo, A., Connors, J., Constantinescu, E., Estep, D., Evans, K., Farhat, C., Hakim, A., Hammond, G., Hansen, G., Hill, J., Isaac, T., Jiao, X., Jordan, K., Kaushik, D., Kaxiras, E., Koniges, A., Lee, K., Lott, A., Lu, Q., Magerlein, J., Maxwell, R., McCourt, M., Mehl, M., Pawlowski, R., Randles, A.P., Reynolds, D., Rivière, B., Rüde, U., Scheibe, T., Shadid, J., Sheehan, B., Shephard, M., Siegel, A., Smith, B., Tang, X., Wilson, C., Wohlmuth, B., 2013. Multiphysics simulations. Int. J. High Perform. Comput. Appl. 27 (1), 4–83. https://doi.org/10.1177/1094342012468181.

Kikuchi, C., 2017. Toward increased use of data worth analyses in groundwater studies.

Gr. Water 55 (5), 670–673. https://doi.org/10.1111/gwat.12562.
Kompala, D.S., Ramkrishna, D., Tsao, G.T., 1984. Cybernetic modeling of microbial growth on multiple substrates. Biotechnol. Bioeng. 26 (11), 1272–1281. https://doi.org/10.1002/bit.260261103.
LaBolle, E.M., Fogg, G.E., Eweis, J.B., Gravner, J., Leaist, D.G., 2008. Isotopic fractionation by diffusion in groundwater. Water Resour. Res. 44 (7), 1–15. https://doi.org/10.1029/2006WR005264.
Lee, L.J.-H., Chung, C.-W., Ma, Y.-C., Wang, G.-S., Chen, P.-C., Hwang, Y.-H., Wang, J.-D., 2003. Increased mortality odds ratio of male liver cancer in a community contaminated by chlorinated hydrocarbons in groundwater. Occup. Environ. Med. 60 (5), 364–369. https://doi.org/10.1136/oem.60.5.364.
Li, Q., Ito, K., Wu, Z., Lowry, C.S., Loheide, S.P., 2009. COMSOL multiphysics: a novel approach to ground water modeling. Gr. Water 47 (4), 480–487. https://doi.org/10.1111/j.1745-6584.2009.00584.x.
Lippmann-Pipke, J., Gerasch, R., Schikora, J., Kulenkampff, J., 2017. Benchmarking PET for geoscientific applications: 3D quantitative diffusion coefficient determination in clay rock. Comput. Geosci. 101, 21–27. https://doi.org/10.1016/j.cageo.2017.01.002.
Lowry, C.S., Loheide, S.P., Moore, C.E., Lundquist, J.D., 2011. Groundwater controls on vegetation composition and patterning in mountain meadows. Water Resour. Res. 47 (10). https://doi.org/10.1029/2010WR010086.
Mackay, D.M., Cherry, J.A., 1989. Groundwater contamination: pump-and-treat remediation. Environ. Sci. Technol. 23 (6), 630–636. https://doi.org/10.1021/es00064a001.
Meckenstock, R.U., Elsner, M., Griebler, C., Lueders, T., Stumpp, C., Aamand, J., Agathos, S.N., Albrechtsen, H.-J., Bastiaens, L., Bjerg, P.L., Boon, N., Dejonghe, W., Huang, W.E., Schmidt, S.I., Smolders, E., Sørensen, S.R., Springael, D., van Breukelen, B.M., 2015. Biodegradation: updating the concepts of control for microbial cleanup in contaminated aquifers. Environ. Sci. Technol. 49 (12), 7073–7081. https://doi.org/10.1021/acs.est.5b00715.
Meckenstock, R.U., Morasch, B., Griebler, C., Richnow, H.H., 2004. Stable isotope fractionation analysis as a tool to monitor biodegradation in contaminated acquifers. J. Contam. Hydrol. 75 (3–4), 215–255. https://doi.org/10.1016/j.jconhyd.2004.06.003.
Moeck, C., Hunkeler, D., Brunner, P., 2015. Tutorials as a flexible alternative to GUIs: an example for advanced model calibration using Pilot Points. Environ. Model. Softw 66, 78–86. https://doi.org/10.1016/j.envsoft.2014.12.018.
Nardi, A., Idiart, A., Trinchero, P., De Vries, L.M., Molinero, J., 2014. Interface COMSOL-PHREEQC (iCP), an efficient numerical framework for the solution of coupled multiphysics and geochemistry. Comput. Geosci. 69, 10–21. https://doi.org/10.1016/j.cageo.2014.04.011.
Nolan, B.T., Malone, R.W., Ma, L., Green, C.T., Fienen, M.N., Jaynes, D.B., Ahuja, L.R., Ma, L., 2011. Inverse modeling with RZWQM2 to predict water quality. In: Ahuja, L.R., Ma, L. (Eds.), Methods of Introducing System Models into Agricultural Research. ASA, CSSA, SSSA, Madison, WI, pp. 327–363.
Obiri-Nyarko, F., Grajales-Mesa, S.J., Malina, G., 2014. An overview of permeable reactive barriers for in situ sustainable groundwater remediation. Chemosphere 111, 243–259. https://doi.org/10.1016/j.chemosphere.2014.03.112.
Palau, J., Yu, R., Hatijah Mortan, S., Shouakar-Stash, O., Rosell, M., Freedman, D.L., Sbarbati, C., Fiorenza, S., Aravena, R., Marco-Urrea, E., Elsner, M., Soler, A., Hunkeler, D., 2017. Distinct dual C-Cl isotope fractionation patterns during anaerobic biodegradation of 1,2-dichloroethane: potential to characterize microbial degradation in the field. Environ. Sci. Technol. 51 (5), 2685–2694. https://doi.org/10.1021/acs.est.6b04998.
Parker, B.L., Chapman, S.W., Guilbeault, M.A., 2008. Plume persistence caused by back diffusion from thin clay layers in a sand aquifer following TCE source-zone hydraulic isolation. J. Contam. Hydrol. 102 (1–2), 86–104. https://doi.org/10.1016/j.jconhyd.2008.07.003.
Parker, R., 1994. Geophysical Inverse Theory. Princeton university press.
Pirnia, P., Duhaime, F., Ethier, Y., Dubé, J.-S., 2018. ICY: an interface between COMSOL multiphysics and discrete element code YADE for the modelling of porous media. Comput. Geosci. https://doi.org/10.1016/j.cageo.2018.11.002.
Ponsin, V., Buscheck, T.E., Hunkeler, D., 2017. Heart-cutting two-dimensional gas chromatography–isotope ratio mass spectrometry analysis of monoaromatic hydrocarbons in complex groundwater and gas-phase samples. J. Chromatogr. A 1492, 117–128. https://doi.org/10.1016/j.chroma.2017.02.060.
Schilling, O.S., Doherty, J., Kinzelbach, W., Wang, H., Yang, P.N., Brunner, P., 2014. Using tree ring data as a proxy for transpiration to reduce predictive uncertainty of a model simulating groundwater-surface water-vegetation interactions. J. Hydrol. 519, 2258–2271. https://doi.org/10.1016/j.jhydrol.2014.08.063.
Schmidt, T.C., Zwank, L., Elsner, M., Berg, M., Meckenstock, R.U., Haderlein, S.B., 2004. Compound-specific stable isotope analysis of organic contaminants in natural environments: a critical review of the state of the art, prospects, and future challenges. Anal. Bioanal. Chem. 378 (2), 283–300. https://doi.org/10.1007/s00216-003-2350-y.
Schreuder, W.A., 2009. Running BeoPEST. In: Proceedings of the 1st PEST Conference.
Scott, C.S., Cogliano, V.J., 2000. Trichloroethylene health risks–state of the science. Environ. Health Perspect. 108 (Suppl. l), 159–160.
Seyedabbasi, M.A., Newell, C.J., Adamson, D.T., Sale, T.C., 2012. Relative contribution of DNAPL dissolution and matrix diffusion to the long-term persistence of chlorinated solvent source zones. J. Contam. Hydrol. 134–135, 69–81. https://doi.org/10.1016/j.jconhyd.2012.03.010.
Sezgin, B., Caglayan, D.G., Devrim, Y., Steenberg, T., Eroglu, I., 2016. Modeling and sensitivity analysis of high temperature PEM fuel cells by using Comsol Multiphysics. Int. J. Hydrog. Energy 41 (23), 10001–10009. https://doi.org/10.1016/j.ijhydene.2016.03.142.
Strang, G., 2016. Introduction to Linear Algebra. Cambridge Press.
Tikhonov, A., Goncharsky, A., Stepanov V, Yagola, A., 2013. Numerical Methods for the Solution of Ill-Posed Problems. Springer.
van Breukelen, B.M., Griffioen, J., 2004. Biogeochemical processes at the fringe of a landfill leachate pollution plume: potential for dissolved organic carbon, Fe(II), Mn (II), NH4, and CH4 oxidation. J. Contam. Hydrol. 73 (1–4), 181–205. https://doi.org/10.1016/j.jconhyd.2004.01.001.
Van Breukelen, B.M., Hunkeler, D., Volkering, F., 2005. Quantification of sequential chlorinated ethene degradation by use of a reactive transport model incorporating isotope fractionation. Environ. Sci. Technol. 39 (11), 4189–4197. https://doi.org/10.1021/es048973c.
Van Breukelen, B.M., Thouement, H.A., Stack, P.E., Vanderford, M., Philp, P., Kuder, T., 2017. Modeling 3D-CSIA data: carbon, chlorine, and hydrogen isotope fractionation during reductive dechlorination of TCE to ethene. J. Contam. Hydrol. 204 (February), 79–89. https://doi.org/10.1016/j.jconhyd.2017.07.003.
Wallis, I., Moore, C., Post, V., Wolf, L., Martens, E., Prommer, H., 2014. Using predictive uncertainty analysis to optimise tracer test design and data acquisition. J. Hydrol. 515, 191–204. https://doi.org/10.1016/j.jhydrol.2014.04.061.
Wanner, P., Parker, B.L., Chapman, S.W., Aravena, R., Hunkeler, D., 2016. Quantification of degradation of chlorinated hydrocarbons in saturated low permeability sediments using compound-specific isotope analysis. Environ. Sci. Technol. 50 (11), 5622–5630. https://doi.org/10.1021/acs.est.5b06330.
Wanner, P., Parker, B.L., Hunkeler, D., 2018. Assessing the effect of chlorinated hydrocarbon degradation in aquitards on plume persistence due to back-diffusion. Sci. Total Environ. 633, 1602–1612. https://doi.org/10.1016/j.scitotenv.2018.03.192.
Wei, H.-Z., Jiang, S.-Y., Xiao, Y.-K., Wang, J., Lu, H., Wu, B., Wu, H.-P., Li, Q., Luo, C.-G., 2012. Precise determination of the absolute isotopic abundance ratio and the atomic weight of chlorine in three international reference materials by the positive thermal ionization mass spectrometer-Cs 2 Cl + -graphite method. Anal. Chem. 84 (23), 10350–10358. https://doi.org/10.1021/ac302498q.
Wei, Z., Weavers, L.K., 2016. Combining COMSOL modeling with acoustic pressure maps to design sono-reactors. Ultrason. Sonochem. 31, 490–498. https://doi.org/10.1016/j.ultsonch.2016.01.036.
Welter, D., White, J., Hunt, R., Doherty, J., 2015. Approaches in Highly Parameterized Inversion— PEST++ Version 3, a Parameter ESTimation and Uncertainty Analysis Software Suite Optimized for Large Environmental Models: U.S. Geological Survey Techniques and Methods. Book 7, Chap. C12. Technical Report. USGS.
White, J.T., Fienen, M.N., Doherty, J.E., 2016. A python framework for environmental model uncertainty analysis. Environ. Model. Softw 85, 217–228. https://doi.org/10.1016/j.envsoft.2016.08.017.
Yang, M., Annable, M.D., Jawitz, J.W., 2017. Field-scale forward and back diffusion through low-permeability zones. J. Contam. Hydrol. 202, 47–58. https://doi.org/10.1016/j.jconhyd.2017.05.001.
Zhou, C., Shao, W., van Westen, C.J., 2014. Comparing two methods to estimate lateral force acting on stabilizing piles for a landslide in the Three Gorges Reservoir, China. Eng. Geol. 173, 41–53. https://doi.org/10.1016/j.enggeo.2014.02.004.
Zou, Z., Shi, Z., 2016. Ship detection in spaceborne optical image with SVD networks. IEEE Trans. Geosci. Remote Sens. 54 (10), 5832–5845. https://doi.org/10.1109/TGRS.2016.2572736.